JOURNAL OF BACTERIOLOGY, Nov. 2002, p. 6280–6288 Vol. 184, No. 22
0021-9193/02/$04.00+0 DOI: 10.1128/JB.184.22.6280–6288.2002

Functional Analysis by Site-Directed Mutagenesis of the NAD^+-Reducing Hydrogenase from *Ralstonia eutropha*

Tanja Burgdorf,[1] Antonio L. De Lacey,[2] and Bärbel Friedrich[1]*

Institut für Biologie, Humboldt-Universität zu Berlin, 10115 Berlin, Germany,[1] and Instituto de Catalisis (CSIC), Campus Universidad Autonoma de Madrid, 28049 Madrid, Spain

Received 20 May 2002/Accepted 16 August 2002

The tetrameric cytoplasmic [NiFe] hydrogenase (SH) of *Ralstonia eutropha* couples the oxidation of hydrogen to the reduction of NAD^+ under aerobic conditions. In the catalytic subunit HoxH, all six conserved motifs surrounding the [NiFe] site are present. Five of these motifs were altered by site-directed mutagenesis in order to dissect the molecular mechanism of hydrogen activation. Based on phenotypic characterizations, 27 mutants were grouped into four different classes. Mutants of the major class, class I, failed to grow on hydrogen and were devoid of H_2-oxidizing activity. In one of these isolates (HoxH I64A), H_2 binding was impaired. Class II mutants revealed a high D_2/H^+ exchange rate relative to a low H_2-oxidizing activity. A representative (HoxH H16L) displayed D_2/H^+ exchange but had lost electron acceptor-reducing activity. Both activities were equally affected in class III mutants. Mutants forming class IV showed a particularly interesting phenotype. They displayed O_2-sensitive growth on hydrogen due to an O_2-sensitive SH protein.

The enzyme hydrogenase catalyzes the reversible cleavage of H_2 into 2 H^+ ions and 2 electrons. Hydrogenases are found in almost all phylogenetic lines of prokaryotes and in a few unicellular eukaryotes. The physiological function of a given hydrogenase is dependent on its cellular location and its capacity to interact with various redox partners. Based on their metal contents, two major classes are distinguished: the [NiFe] and Fe-only hydrogenases. Fe-only hydrogenases are extremely sensitive to O_2 and so far have been found only in obligate anaerobes, where they occur either as a monomer in the cytoplasm or as a heterodimer in the periplasm (1, 45). [NiFe] hydrogenases are composed of at least two heterologous polypeptides, a large subunit of approximately 60 kDa and a small subunit that is relatively diverse in size and cofactor composition (40).

Crystallographic data are available for both classes of hydrogenases (12, 15, 16, 25, 27, 42). An X-ray structure was first obtained for the periplasmic [NiFe] hydrogenase of *Desulfovibrio gigas*, which was thereafter considered a prototypic hydrogenase. The active site of an [NiFe] hydrogenase is deeply buried inside the protein. It consists of a heterobinuclear metal center which is coordinated to the protein by 4 cysteines (42). Further refinement and isotopic substitution coupled with infrared spectroscopy revealed the presence of three nonprotein ligands, 1 CO and 2 CN^- molecules, bound to the Fe (4, 14, 28, 38, 41). This unusual architecture of the active site may account for a relatively high O_2 tolerance of [NiFe] hydrogenases. The small subunit of a standard [NiFe] hydrogenase contains three [Fe-S] clusters which obviously participate in the electron transfer between the active [NiFe] site and the protein surface. Despite a great wealth of biochemical and biophysical information, the precise mechanism of the reaction of [NiFe] hydrogenases with H_2 remains a matter of dispute. Electron paramagnetic resonance (EPR) spectroscopy and X-ray absorption spectroscopy (XAS) show that H_2 activation occurs close to the nickel atom, suggesting a change in its oxidation state during the catalytic cycle (14, 26, 39).

Mutant proteins are useful tools for mechanistic studies. A complex protein-assisted maturation pathway is involved in the assembly of the [NiFe] active site (7, 17, 19). Almost no information is available on these posttranslational processes in strictly anaerobic organisms, whose hydrogenase structure is well defined. On the other hand, elaborate efforts to crystallize [NiFe] hydrogenases from aerobic organisms, for which hydrogenase biosynthesis has been extensively studied, have not yet been successful.

More than 100 hydrogenase gene sequences are now available in the database. Inspection of these sequences shows that despite functional and structural diversity, core signatures are highly conserved in the catalytic subunit, in particular in the environment of the [NiFe] active site (3, 43). Therefore, analysis of mutant proteins, in correlation with the available atomic structures, should provide further insight into the reaction mechanism of [NiFe] hydrogenases.

In this study we selected the cytoplasmic [NiFe] hydrogenase (soluble hydrogenase [SH]) of *Ralstonia eutropha* as a model. This hydrogenase consists of a heterodimeric hydrogenase module together with a flavin mononucleotide (FMN)-containing iron-sulfur protein, in which the capacity to couple H_2 oxidation with the reduction of NAD^+ resides (21, 32, 33). The SH is highly insensitive to oxygen and carbon monoxide (31), properties which might be related to the presence of two extra CN^- ligands at the active site (13). Both redox moieties of the SH have extensive similarity to the mitochondrial and bacterial NADH-ubiquinone oxidoreductases (2, 29).

In a previous study Massanz and Friedrich (20) constructed SH mutants by amino acid replacements in three of six conserved motifs surrounding the active site. They demonstrated that only three of the four Ni-ligating cysteine residues are

* Corresponding author. Mailing address: Institut für Biologie, Humboldt-Universität zu Berlin, Chausseestrasse 117, 10115 Berlin, Germany. Phone: (49) 30 2093 8101. Fax: (49) 30 2093 8102. E-mail: baerbel.friedrich@rz.hu-berlin.de.

TABLE 1. Strains and plasmids

Strain or plasmid	Relevant characteristics[a]	Source or reference
Strains		
R. eutropha		
H16	SH^+ MBH^+	DSM 428, ATCC 17699
HF424	SH^- MBH^-	21
E. coli S17-1	*recA pro thi hsdR chR*::RP4-2 Tra^+	34
Plasmids		
pBluescript KS(+)	Ap^r *lacZ′* T7 ϕ10 promoter f1*ori*	Stratagene, cloning system
pCH472	1.9-kb *Sst*I fragment of pGE15 in pBluescript KS(+)	22
pGE15	15.0-kb *Hin*dIII fragment of pHG1 in pVK101	37
pGE331	Derivative of pGE15 with a 1.9-kb *Sst*I fragment deleted	22

[a] MBH, membrane-bound hydrogenase.

essential for nickel incorporation, and they identified a mutant in which electron transfer is blocked although the proton flow remains unaffected. In this report we extend the site-directed mutagenesis to all six conserved regions of the active site-containing subunit HoxH. The resulting SH mutants were characterized with respect to their catalytic and structural properties, taking into account the modified composition of the [NiFe] cofactor (13) and the recent observations that intramolecular channels exist which direct the gases to the catalytic center (10, 24).

MATERIALS AND METHODS

Bacterial strains and growth conditions. The bacterial strains and plasmids used in this study are listed in Table 1. Strains whose designations begin with the letters "HF" are derived from *R. eutropha* H16 harboring the endogenous megaplasmid pHG1. *R. eutropha* strains were cultivated in mineral salts medium containing 0.4% (wt/vol) fructose or a mixture of 0.2% (wt/vol) fructose and 0.2% (vol/vol) glycerol (FGN medium) (11). Under standard conditions the medium was supplemented with 1 μM $NiCl_2$. Lithoautotrophic cultures were grown on mineral salts medium under an atmosphere of H_2, CO_2, and O_2 (8:1:1, vol/vol/vol). *Escherichia coli* strains were cultivated in Luria-Bertani medium (23). Antibiotics were added to a final concentration of 20 μg/ml (tetracycline) or 100 μg/ml (ampicillin).

Recombinant DNA techniques. Standard DNA techniques were used (30). Site-directed mutations in *hoxH* were constructed by a two-step PCR with plasmid pCH472 as the template (20). A 194-bp *Bst*EII-*Sty*I fragment was used to introduce alterations in motifs L0 and L2. Likewise, a 211-bp *Sty*I-*Xcm*I fragment, a 208-bp *Pfl*MI-*Bsm*I fragment, or a 309-bp *Bsm*I-*Bcl*I fragment was used to generate mutations in L3, L4, or L5, respectively. The exchanges were verified by double-stranded sequencing of the corresponding inserts. Cycle sequencing was performed with internal infrared-labeled primers by using the SequiTherm Excel II sequencing kit (Biozym, Hessisch Oldendorf, Germany). As described previously (20), the mobilizable plasmid pGE331 was used to generate recombinant plasmids for complementation studies. The resulting plasmids were transferred from *E. coli* S17-1 cells to *R. eutropha* HF424 cells (SH^- MBH^-) by agar spot mating (9). Transconjugants were selected on fructose minimal medium containing tetracycline.

Activity measurements. *R. eutropha* cells were grown in FGN medium to an optical density of 11 at 436 nm. Cells were harvested by centrifugation, washed once, and resuspended in 50 mM potassium phosphate buffer (pH 7) containing 0.1 mM phenylmethylsulfonyl fluoride. After two passages through a chilled French pressure cell at 900 lb/in^2 (6.2 MPa), soluble extracts were prepared by ultracentrifugation (at 100,000 × *g* for 30 min). Protein concentrations were determined by the method of Bradford (5) with bovine serum albumin as a reference. The hydrogenase activity of the SH was assayed with soluble fractions by monitoring the reduction of NAD^+ or benzyl viologen (BV) in the presence of H_2. The NADH oxidoreductase (diaphorase) activity was measured with NADH as the electron donor and BV as the electron acceptor (33). Deuterium-proton (D_2/H^+) exchange experiments were performed as described previously (22).

^{63}Ni autoradiography and immunological studies. ^{63}Ni-labeled proteins were prepared by growing *R. eutropha* cells in FGN medium in the presence of 150 nM $^{63}NiCl_2$ (867 mCi/mmol). Soluble extracts were analyzed by native polyacrylamide gel electrophoresis (PAGE) and autoradiography (8). For immunoblot analysis, proteins were separated in polyacrylamide gels and transferred to nitrocellulose membranes (Biotrace NT, Pall, Mich.) according to a standard protocol (36). The HoxH subunit was detected with a rabbit polyclonal antiserum prepared against the individual subunit and an alkaline phosphatase-labeled goat anti-rabbit immunoglobulin (Dianova, Hamburg, Germany).

RESULTS

Amino acid replacements in HoxH, the active-site-containing subunit of the SH. The active-site-containing subunit of [NiFe] hydrogenases reveals five short signatures of highly conserved amino acids, defined as L1 to L5 (Fig. 1) (3, 43). A large number of [NiFe] hydrogenases contain an additional conserved motif, consisting of mostly charged residues (RxEGH) positioned close to the N terminus (Fig. 1), referred to here as motif L0. The two pairs of Ni-Fe-coordinating cysteines reside in motifs L2 and L5. It is notable that almost all of the conserved residues appear to be located in the environment of the active site, as illustrated in Fig. 4A.

Some SH mutants of *R. eutropha* with alterations in motif L1, L2, or L5 of the HoxH protein have been characterized recently (20). In the present study we introduced mutations in motifs L0, L3, and L4 of HoxH and changed additional residues in motifs L2 and L5, as listed in Fig. 1. Site-directed mutagenesis was conducted by using a two-step PCR. The modified *hoxH* alleles (Table 2) were introduced into the broad-host-range plasmid pGE15, which carries the four SH genes *hoxFUYH* in addition to the endopeptidase gene *hoxW* and four SH-linked accessory genes whose products are involved in the posttranslational maturation of the SH (35, 44). The recombinant plasmids were finally transferred to *R. eutropha* HF424 by conjugation. The recipient strain HF424 is unable to grow on H_2 due to deletions in the genes coding for the SH and the membrane-bound hydrogenase (21). By use of this strain, undesired interference with the wild-type hydrogenases was excluded.

Growth characteristics of the SH mutants. The newly constructed mutants were first investigated for growth under autotrophic conditions with H_2 as the sole energy source. Of the 27 strains tested, 14 mutants had lost the capacity to grow on H_2 (Table 3). The remaining strains maintained the ability to

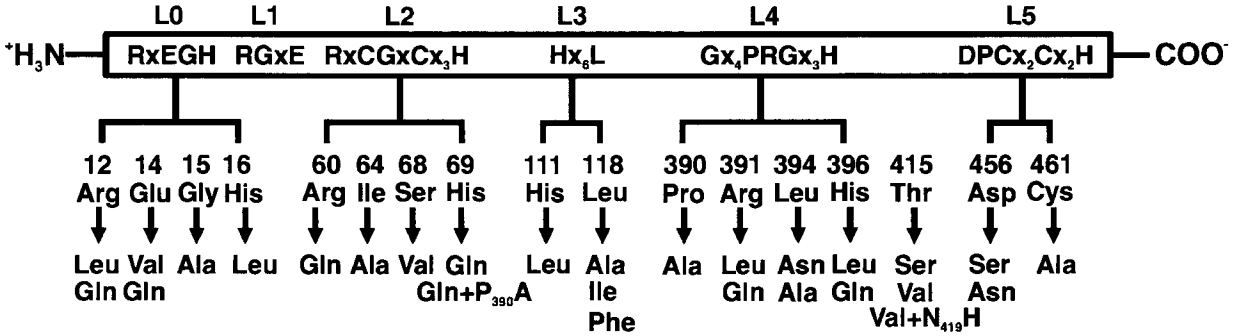

FIG. 1. Consensus motifs (L0 to L5) in the HoxH polypeptide of *R. eutropha*. The positions of the amino acid residues which were replaced by mutation are given below the diagram.

grow on H_2, indicating a catalytically active SH. The growth pattern of the mutants, however, differed widely. Based on growth rates on H_2, four phenotypes were distinguished: (i) near-wild-type derivatives exhibiting a doubling time (t_d) of approximately 4.5 h, (ii) growth-retarded strains with a t_d between 5 and 6.8 h, (iii) extremely poorly growing mutants with a t_d longer than 8 h, and finally (iv) strains which failed to grow on H_2.

Enzymatic properties. To investigate the enzymatic properties of the mutants in further detail, SH assays were performed with soluble extracts prepared from cells cultivated heterotrophically under hydrogenase-derepressing conditions (11). Since the SH is composed of two distinct redox modules (21), its catalytic activity can be traced by module-specific assays in addition to the overall reaction yielding NADH, mediated by the SH tetramer. Reactions catalyzed by the hydrogenase dimer were followed by H_2-coupled reduction of the redox dye BV and by D_2/H^+ exchange. The latter reaction proceeds without an electron transfer process. The Fe-flavoprotein moiety displays diaphorase activity, which was determined by oxidation of NADH with BV as the electron acceptor.

TABLE 2. Mutant *hoxH* alleles in derivatives of pGE15

Plasmid	pBluescript cloning intermediate	Codon change(s)	Amino acid exchange
pGE468	pCH884	CGC→CTG	R12L
pGE469	pCH885	CGC→CAG	R12Q
pGE470	pCH886	GAG→GTC	E14V
pGE471	pCH887	GAG→CAG	E14Q
pGE472	pCH888	GGT→GCG	G15A
pGE473	pCH889	CAC→CTC	H16L
pGE474	pCH890	CGC→CAG	R60Q
pGE475	pCH891	ATC→GCC	I64A
pGE476	pCH892	AGT→GTG	S68V
pGE477	pCH893	CAC→CAG	H69Q
pGE478	pCH894	CAC→CAG, CCA→GCG	H69Q + P390A
pGE480	pCH896	CTG→GCC	L118A
pGE481	pCH897	CTG→ATC	L118I
pGE482	pCH898	CTG→TTC	L118F
pGE483	pCH899	CCA→GCG	P390A
pGE484	pCH900	CGC→CTG	R391L
pGE485	pCH901	CGC→CAG	R391Q
pGE486	pCH902	TTG→GCG	L394A
pGE487	pCH903	TTG→AAT	L394N
pGE488	pCH904	CAC→CTG	H396L
pGE489	pCH905	CAC→CAG	H396Q
pGE490	pCH906	GAT→TCG	D456S
pGE491	pCH907	GAT→AAC	D456N
pGE492	pCH908	TGC→GCC	C461A
pGE493	pCH909	ACC→TCG	T415S
pGE494	pCH910	ACC→GTG	T415V
pGE495	pCH911	ACC→GTG, CAA→ACA	T415V + N419H

TABLE 3. Growth of strains carrying mutated *hoxH* alleles

Amino acid exchange(s) in HoxH[a]	t_d (h)[b]	Conserved motif
SH^- MBH^-	NG	
SH^- MBH^-	4.5	
R12L	NG	L0
R12Q	NG	
E14V	NG	
E14Q	NG	
G15A	NG	
H16L	NG	
R60Q	9.3	L2
I64A	NG	
S68V	6.8	
H69Q	6.0	
H69Q + P390A	6.7	
L118A	6.7	L3
L118I	5.1	
L118F	NG	
P390A	5.3	L4
R391L	NG	
R391Q	NG	
L394N	NG	
L394A	4.1	
H396L	8.9	
H396Q	5.6	
D456S	NG	L5
D456N	NG	
C461A	NG	
T415S	5.4	Nonconserved residues
T415V	6.4	
T415V + N415H	6.0	

[a] HoxH is the catalytic-site-containing subunit of the SH. MBH, membrane-bound hydrogenase.

[b] Cells were cultivated in mineral salts medium under an atmosphere of 10% O_2, 10% CO_2, and 80% H_2. NG, no growth.

TABLE 4. Enzymatic activities of SH mutant proteins

Amino acid exchange(s) in HoxH[a]	Activity (%)[b]				Conserved motif
	H_2-NAD^+	H_2-BV	D_2/H^+	NADH-BV	
SH^+	100	100	100	100	
SH^- MBH^-[c]	<0.5	0	0.00	6.1	
R12L	3.0	<0.5	1.2	39.2	L0
R12Q	1.7	<0.5	0.6	65.9	
E14V	<0.5	0.5	0	80.9	
E14Q	0.0	<0.5	0	96.2	
G15A	<0.5	<0.5	0	63.1	
H16L	4.7	7.4	64.2	79.3	
R60Q	2.2	17.1	68.5	98.7	L2
I64A	2.4	2.5	1.8	109.6	
S68V	3.5	6.0	19.4	78.7	
H69Q	20.6	23.1	59.4	54.5	
H69Q + P390A	16.2	9.0	31.5	64.3	L3
L118A	60.3	51.3	38.8	82.3	
L118I	69.4	68.3	91.5	80.6	
L118F	25.2	26.1	8.5	88.2	
P390A	20.1	24.6	27.9	81.5	L4
R391L	0	<0.5	0	56.4	
R391Q	0	<0.5	0	35.7	
L394N	<0.5	0.5	0	31.5	
L394A	20.4	3.5	17.6	15.3	
H396L	9.6	9.1	17.6	58.9	
H396Q	29.7	31.2	34.5	47.4	
D456S	<0.5	<0.5	0	43.6	L5
D456N	<0.5	<0.5	ND[d]	41.0	
C461A	0	<0.5	0	36.4	
T415S	18.1	16.6	11.5	30.3	Nonconserved residues
T415V	3.9	9.0	27.9	34.7	
T415V + N419H	3.2	1.5	21.2	53.2	

[a] Cells were grown under heterotrophic hydrogenase-derepressing conditions in fructose-glycerol medium (11).

[b] Activities of the SH^+ strain HF424(pGE15) were set at 100%. Data are averages from at least three independent experiments, with variation of less than 25%. Maximal H_2 oxidation activities were 5.9 U/mg (H_2-NAD^+) and 2.0 U/mg (H_2-BV). The maximal D_2-H^+ exchange rate was 1.7 U/mg. The maximal level of NADH-dependent BV reduction was 3.1 U/mg.

[c] MBH, membrane-bound hydrogenase.

[d] ND, not determined.

All mutants showed decreases in the H_2 oxidation rate, although to various extents (Table 4). Significant amounts of H_2-NAD^+-reducing activity, ranging from 16 to almost 70%, were found in nine derivatives carrying the following amino acid substitutions: H69Q, H69Q + P390A, L118I, L118A, L118F, P390A, L394A, H396Q, and T415S. In most cases the H_2-NAD^+ activity correlated well with the H_2-BV activity and the D_2/H^+ exchange rate. Three mutants (the H16L, R60Q, and H69Q mutants), however, showed high D_2/H^+ exchange rates (59 to 69%) and relatively low H_2 oxidoreductase activities (below 21%).

It is interesting that the growth behavior of two of the mutants (the S68V and T415V + N419H mutants) was not severely affected, in spite of their low H_2 oxidoreductase activities (Tables 3 and 4). On the other hand, the L118F mutant, which completely failed to grow on H_2, still exhibited 25% of wild-type H_2-coupled NAD^+-reducing activity. These apparent discrepancies will be discussed below.

Without a single exception, the mutants contained NADH-BV activity (Table 4). This observation is consistent with the notion that the SH is properly expressed and relatively stable, at least so far as the diaphorase module is concerned. In some instances (the E14V, E14Q, H16L, R60Q, I64A, S68V, L118A, L118I, L118F, and P390A mutants), more than 78% of diaphorase activity was recovered, which indicates that a severe lesion in the H_2-converting moiety does not necessarily affect the activity and stability of the NADH oxidoreductase module. Almost half of the mutants tested, however, showed >50%-decreased diaphorase activity, indicating an increased instability of the modified protein.

Maturation and oligomerization state of the mutant proteins. Biosynthesis of hydrogenases is a multistep protein-assisted process (19). Ni insertion and assembly of the [NiFe] active site into the SH of *R. eutropha* involve the function of seven *hyp* gene products (6, 8, 44). Hence, maturation is completed by the proteolytic removal of 24 amino acids from the C terminus of HoxH mediated by the endopeptidase HoxW, which triggers the oligomerization of the protein (22).

To gain further insights into the nature of catalytically inactive SH mutant proteins, we examined the following parameters: Ni incorporation, C-terminal processing, and the stability of the SH (Fig. 2). In vivo Ni incorporation was monitored by ^{63}Ni autoradiography using a standard protocol (8). Mutant cells were cultivated heterotrophically in the presence of $^{63}NiCl_2$, and soluble extracts derived from them were subjected to native PAGE. The monomeric HoxH polypeptide could be distinguished from the tetrameric SH protein by its rapid migration (Fig. 2A). The authenticity and the stability of the respective proteins were documented in a parallel Western blot experiment (data not shown). A stable Ni-containing SH tetramer was observed with two mutants, I64A (Fig. 2A, lane 6) and H16L (lane 11). The ^{63}Ni-labeled HoxH monomer was identified in four mutant extracts (from the E14V [lane 3], G15A [lane 4], C461A [lane 7], and R12L [lane 10] mutants). It is interesting that in these cases, as well as for mutant protein D456S (Fig. 2A, lane 8), Ni-labeled subforms occurred, presumably due to dissociation of the holoenzyme. Two mutants (the R391L [lane 5] and L394N [lane 9] mutants) showed no SH-related Ni signal and no SH-specific antigen (data not shown), indicating a high degree of protein instability. Western blot analysis of sodium dodecyl sulfate-treated extracts demonstrated that the HoxH subunits of the stably expressed mutant proteins were proteolytically processed (data not shown). From these results we conclude that only a small fraction of the mutants which are completely devoid of catalytic SH activity are able to form a stable tetramer.

Oxygen-sensitive mutants. One of the outstanding features of the SH is its O_2 tolerance, which is presumably attributable to an extra CN^- bound to the Ni atom (13). The apparent discrepancy between the growth rate on H_2 and the enzymatic SH activity observed for some mutant strains (Tables 3 and 4) prompted us to investigate their behavior toward O_2.

Under standard lithoautotrophic conditions, the gas atmosphere contains a mixture of 80% H_2, 10% O_2, and 10% CO_2. Increasing (15%) or decreasing (5%) the amount of O_2 did not affect the growth of wild-type *R. eutropha* (Fig. 3). Some of the

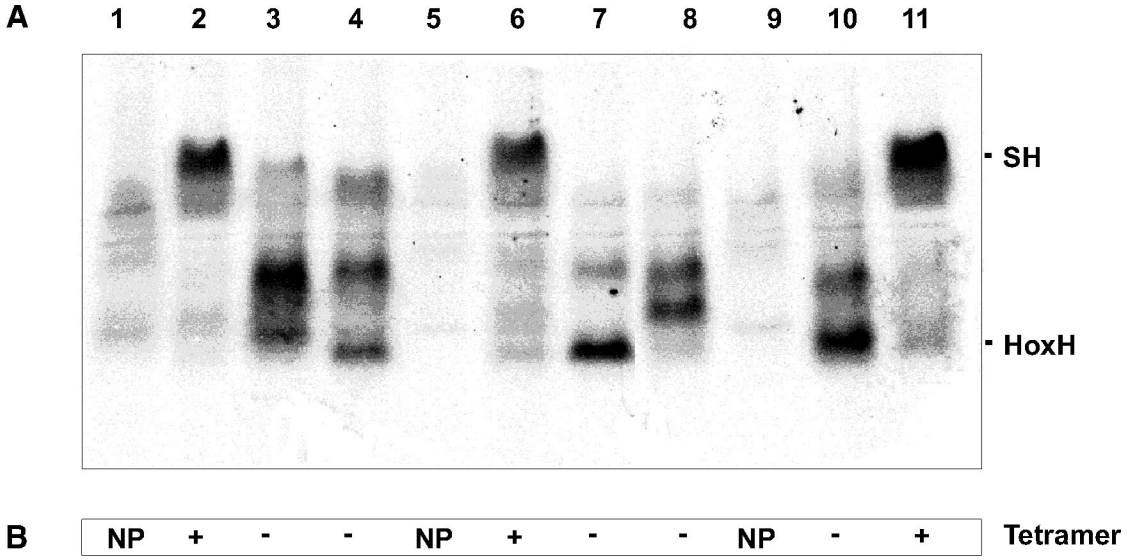

FIG. 2. SH maturation state in selected mutant strains. Mutations (strains) are as follows: lane 1, SH^- (HF424); lane 2, SH^+ [HF424(pGE15)]; lane 3, E14V; lane 4, G15A; lane 5, R391L; lane 6, I64A; lane 7, C461A; lane 8, D456S; lane 9, L394N; lane 10, R12L; lane 11, H16L. (A) ^{63}Ni incorporation in vivo, demonstrated by autoradiography. Cells were grown in the presence of 150 nM $^{63}NiCl_2$. Portions (100 μg) of soluble extracts were separated by native PAGE (4 to 15% acrylamide). (B) Analysis of SH assembly by immunoblotting with anti-HoxH antibodies after native PAGE (data not shown). NP, no protein signal detectable; +, the tetrameric SH enzyme was present; −, no SH holoenzyme could be found.

mutants, however, responded to varying concentrations of O_2 very sensitively. The L118F mutant showed growth neither at 10% nor at 15% O_2 (Tables 3 and 5), but slow growth occurred at 5% O_2 (Fig. 3). The R60Q mutant grew at near-wild-type rates at an O_2 concentration of 5% but showed significant retardation at 10% O_2 (Tables 3 and 5) and 15% O_2 (Fig. 3). Another O_2-related phenomenon was observed with the T415V N419H double mutant. At high O_2 concentrations this strain exhibited an extensive lag phase (Fig. 3). When growth resumed, however, its rate was almost equivalent to that of the wild type (Tables 3 and 5).

A collection of mutant strains which displayed O_2-sensitive lithoautotrophic growth was further tested for an effect of O_2 on SH activity in vitro (Table 5). Under standard conditions NAD^+ reduction is assayed in an H_2-saturated buffer. To obtain an estimate of whether the presence of O_2 in the reaction

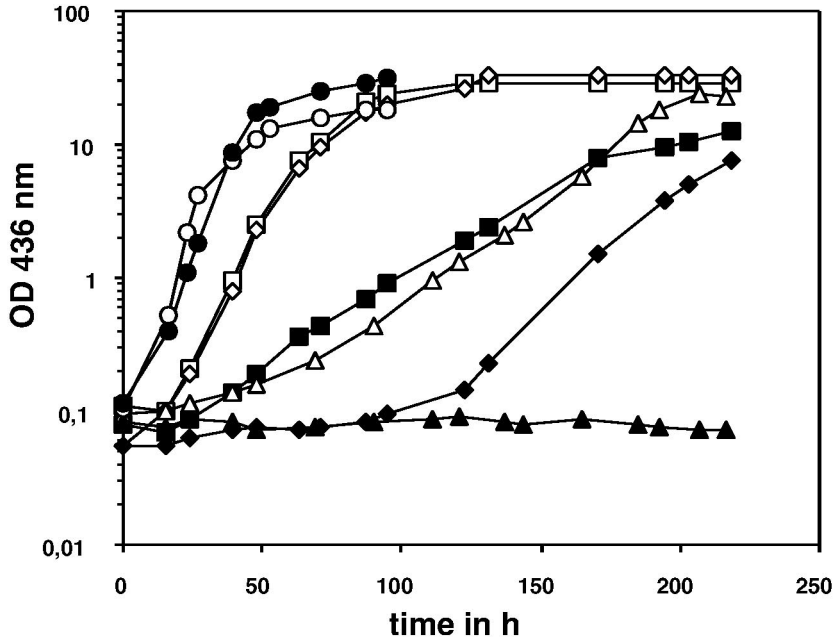

FIG. 3. Autotrophic growth on H_2 at varying oxygen concentrations. Cells were cultivated in the presence of 75% (vol/vol) H_2, 10% (vol/vol) CO_2, and 5 or 15% (vol/vol) O_2. N_2 was added to give a total of 100%. Open symbols, cultivation with 5% O_2; solid symbols, cultivation with 15% O_2; circles, wild type; squares, R60Q mutant; triangles, L118F mutant; diamonds, T415V N419H double mutant.

TABLE 5. H_2-NAD^+ activities of mutant proteins exhibiting different O_2 sensitivities

Amino acid exchange(s)	t_d (h) at the following O_2 concn[a]:		H_2-NAD^+ activity (%)[b] at:		
	5%	15%	100% H_2	20% N_2	20% O_2
SH^+	4.3	4.5	100.0	98.4	96.3
R60Q	7.0	22.2	2.2	2.2	0.9
S68V	5.4	10.2	3.5	3.2	3.6
L118F	15.2	NG	25.2	26.1	13.1
H396L	6	34.5	9.6	9.4	6.0
T415V + N419H	7.4	14.4	3.2	3.3	1.8

[a] The growth rate under lithoautotrophic conditions (75% H_2, 10% CO_2) in the presence of 5 or 15% oxygen (N_2 was added to 100%) was determined. NG, no growth.
[b] The standard activity assay was performed in an H_2-saturated buffer. The resulting activity of each strain was set at 100%. An appropriate volume of the N_2- or O_2-saturated buffer was added to the reaction mixture to obtain a final concentration of 20%. The maximal H_2-NAD^+ activity under hydrogen saturation was 5.9 U/mg in the SH^+ strain HF424(pGE15).

TABLE 6. Classification of the mutants

Class	Mutants	Major characteristics
I	R12L, R12Q, E14V, E14Q, G15A, I64A, R391L, R391Q, L394N, D456S, D456N, C461A	No growth on H_2; no H_2-BV or D_2/H^+ activity; SH holoenzyme destabilized[a]
II	H16L, S68V, H69Q, T415V	Variable growth pattern on H_2; high D_2/H^+ exchange rate relative to the H_2-BV activity
III	H69Q + P390A, L118A, L118I, P390A, L394A, H396Q, T415S	Variable growth pattern on H_2; D_2/H^+ exchange rate corresponds to the H_2-oxidizing activity
IV[b]	R60Q, L118F, H396L, T415V + N419H	O_2-sensitive growth on H_2; O_2-sensitive H_2-NAD^+ activity

[a] Except for the 164A mutants for which a stable SH holoenzyme was detected.
[b] A class of O_2-sensitive isolates comprising mutants otherwise similar to members of class II (the R60Q and T415V + N419H mutants) and III (the L118F and H396L mutants).

mixture leads to further decreases in SH activity, 20% N_2- or O_2-saturated buffer was added. Of five mutant extracts tested, four SH proteins showed 30%- to 50%-lower activity when exposed to O_2 during the assay. This result is in accordance with the assumption that in this class of mutants the O_2 tolerance of the SH is significantly reduced. Since the extracts were prepared with cells cultivated heterotrophically to high cell densities where the O_2 tension is presumably rather low, residual amounts of SH activity were still detected in the mutant strains (Table 4).

DISCUSSION

Phenotypic characterization of site-directed mutants carrying amino acid replacements in the [NiFe] cofactor-containing subunit HoxH of the SH from *R. eutropha* yielded four different classes of mutants. This classification was based on H_2-dependent growth, module-specific enzymatic activity, immunological analysis, and in vivo incorporation of $^{63}Ni^{2+}$.

The majority of the 27 mutants tested fell into class I (Table 6). These mutants were virtually devoid of H_2-oxidizing activity including D_2/H^+ exchange and hence failed to use H_2 for growth. The SH holoenzyme was intact only in one isolate (the I64A mutant), suggesting that the mutations introduced at these sites of HoxH had a rather destructive effect on the conformation and stability of the SH protein.

Class II mutants (Table 6) comprised strains that displayed a high D_2/H^+ exchange rate but a moderate or low H_2-BV-reducing activity. In fact, the H16L isolate phenotypically resembled the R40L mutant, characterized previously as being active in proton exchange but inactive in electron transfer (20).

In class III mutants (Table 6), the H_2-oxidizing activity and the D_2/H^+ exchange rate were equally affected. Activity levels in these mutants correlated with decreased growth rates. The especially interesting class IV contained mutants initially grouped into classes II and III (Table 6). These four strains displayed O_2-sensitive chemolithoautotrophic growth as a result of an O_2-sensitive SH protein.

What do we learn if we correlate the phenotypic characteristics of the mutant proteins with the atomic structure of a standard [NiFe] hydrogenase? Figure 4A schematically shows that the six motifs (L0 through L5) are positioned close to the [NiFe] active site in the *D. gigas* hydrogenase (42). This part of the protein is highly conserved in the amino acid sequence of HoxH (37). Thus, despite the fact that the SH is a tetrameric protein which presumably shares only the proximal [Fe-S] cluster of the small electron-transferring subunit HoxY, biochemical analysis of the SH mutant proteins promises new insights into the catalytic process.

In class I mutants, motifs L0, L2, L4, and L5 were altered. Motif L5 harbors the C-terminal pair of cysteines, which participates in the coordination of the metals. As shown previously, replacement of C458 by Ser abolished Ni incorporation, whereas an exchange at the distal Cys461, which correlates with the bridging ligand Cys533 in the *D. gigas* enzyme, still allowed Ni binding to HoxH and C-terminal proteolysis (20). The fact that the newly constructed C461A mutant behaved identically excludes the possibility that the metal in C461S is coordinated via the hydroxyl group of serine. This result is in agreement with a mutant phenotype described for hydrogenase 3 of *E. coli* (18). The lack of enzymatic activity and the inability of the C461 mutants to form an oligomeric holoenzyme suggest that the distal Cys is absolutely necessary for accurate maturation of the SH. The same pertains to D456, which has been proposed to be directly involved in the assembly of the [NiFe] center. A D456V exchange mutant was enzymatically inactive and contained only a residual amount of Ni in the HoxH subunit (20). In the newly constructed D456S mutant, Ni-labeled subforms were detected. This observation emphasizes that a polar residue at this position is necessary for structural reorganization during cofactor insertion. The aspartate side chain, however, is indispensable for the formation of a stable SH holoenzyme.

I64, the conserved hydrophobic residue of motif L2, is located between the two N-terminal cysteines which provide thiol ligands for the active site. In *D. gigas* the corresponding

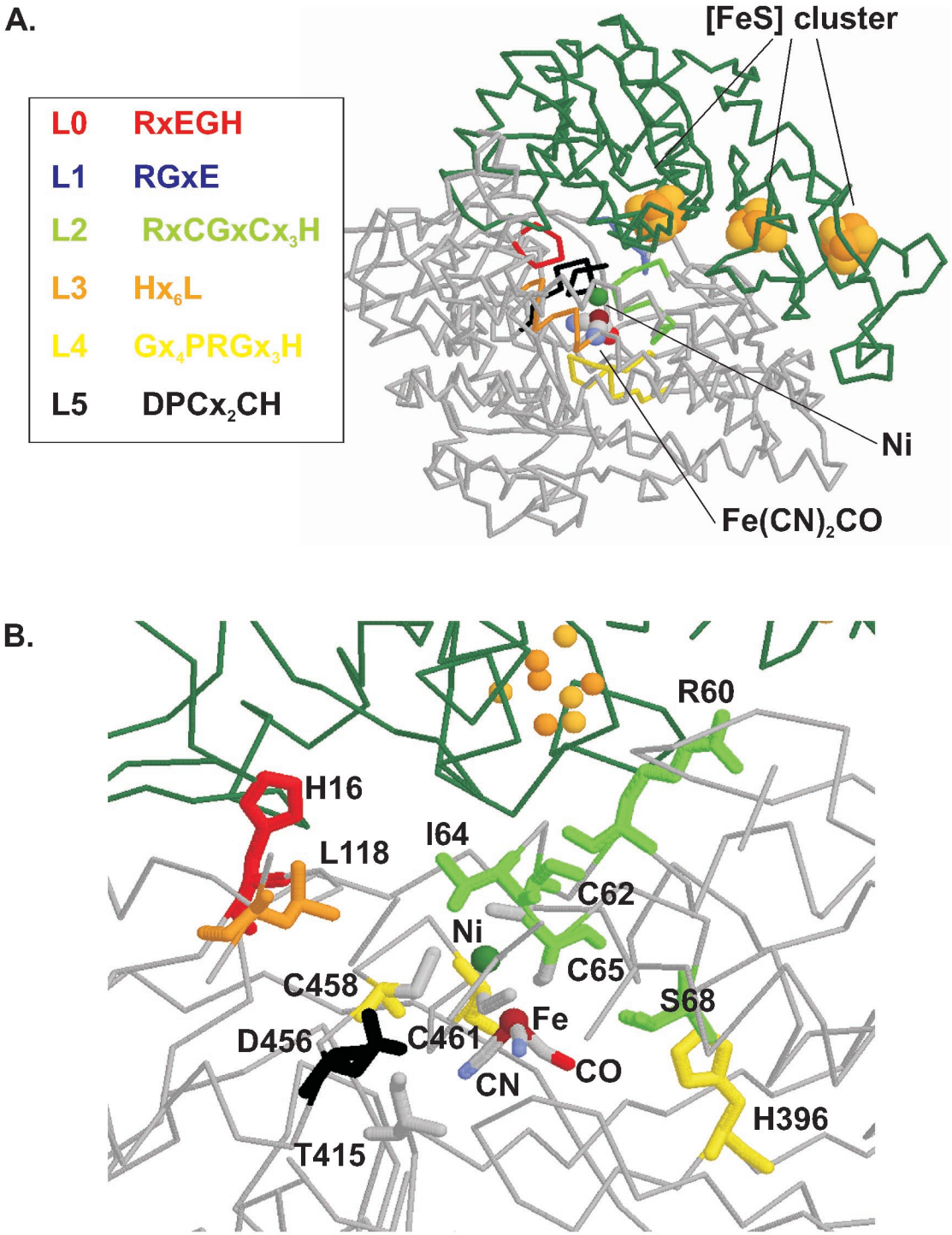

FIG. 4. Schematic representation of the crystal structure of the periplasmic [NiFe] hydrogenase from *D. gigas*. (A) General overview. The coordinates (2frv) were taken from the Brookhaven Protein Data Bank. The Cα backbone of the large subunit is drawn in grey, and that of the small subunit is drawn in green. The six conserved motifs and their positions in the catalytic subunit are represented in different colors (red, L0; green, L2; orange, L3; yellow, L4; black, L5). The [NiFe] center with the diatomic ligands and the proximal [4Fe-4S] cluster are depicted by ball-and-stick representation. (B) Close-up view of the *D. gigas* [NiFe] hydrogenase active site. The side chains of selected residues that were mutated in *R. eutropha* are drawn as sticks. Numbering of residues refers to the HoxH coordinates of *R. eutropha*. These residue numbers, with the corresponding residues of the *D. gigas* hydrogenase (41, 42) given in parentheses, are as follows: H16 (H20), R60 (R63), C62 (C65), I64 (V67), C65 (C68), S68 (V71), L118 (L115), H396 (H468), T415 (S486), C458 (C530), and C461 (C533).

residue (V67) covers the Ni (Fig. 4B; distance from Cγ1 or Cγ2 to Ni, 5.1 or 5.3 Å, respectively) and was thus proposed to extend the hydrophobic cavities identified by Xe labeling (24). The results obtained in this study indicate that the I64A mutant was impaired in H_2 binding. Thus, it is conceivable that the isoleucine may indeed be part of a hydrophobic channel leading H_2 to the active site, a process that might be interrupted by the alanine replacement.

According to the X-ray structure, residues of motif L0 are positioned near the interface with the small subunit (Fig. 4A) and therefore are candidates for direct interactions between the two subunits. Furthermore, E18 in *D. gigas* has been postulated to be involved in proton transfer (10). In the *R. eutropha* SH, however, not only the corresponding conserved glutamate E14 but also R12 and G15 are indispensable for the structural integrity of the SH protein. Exchange of residue H16 in L0 did not destroy the oligomeric conformation of the SH. Nevertheless, H_2 oxidoreductase activity was completely abolished in this class II mutant, whereas the D_2/H^+ exchange rate was less affected. This observation indicates that H16, like the previously described R40 located in motif L1 (20), is important for maintaining a structure which allows the transfer of electrons from the active site to the proximal electron acceptor.

The less-conserved amino acid S68 of L2 is replaced by valine in several hydrogenase sequences. In *D. gigas* V71 is located in the vicinity of the [NiFe] center (Fig. 4B; distance from Cγ2 to Ni, 6.5 Å; distance from Cγ2 to Fe, 4.8 Å), pointing with its second Cγ-atom toward the oxygen of the CO ligand (distance from Cγ2 to O, 3.6 Å). Replacement of S68 in HoxH by a more-hydrophobic valine resulted in an SH protein with a low H_2 oxidation rate. These results suggest that S68 may be involved in the stabilization of the extra CN^- at the Fe atom which has been identified in the SH by Fourier transform infrared microscopy spectroscopy (13).

Previous studies showed that replacement of R60 by leucine still allowed nickel incorporation but impaired oligomerization of the SH and abolished its H_2-oxidoreductase activity (20). In this study we replaced R60 of motif L2 by a glutamine residue and obtained a mutant protein with a relatively high D_2/H^+ exchange rate which was O_2 sensitive. The corresponding residue in the *D. gigas* hydrogenase (R63) is close to the proximal [4Fe-4S] cluster (Fig. 4B). Thus, the low H_2 oxidation rate of R60Q in combination with its O_2 sensitivity may reflect the fact that R60 is not only involved in subunit interaction but also contributes to stability in the presence of O_2.

The L118F isolate, in which motif L3 is altered, also displayed an O_2-sensitive phenotype. In *D. gigas* the corresponding leucine residue is approximately 10 Å away from the active site (Fig. 4B; distance from Cδ2 to Ni, 9.4 Å). This leucine is widely conserved in energy-coupled hydrogenases, whereas in H_2-sensing proteins, phenylalanine substitutes for leucine. In the case of the SH, the extra CN^- ligand at the Ni appears to account for the high O_2 tolerance and the lack of sensitivity to CO (13). It is attractive to postulate that the bulky phenylalanine blocks the incorporation of the extra ligand on the Ni and confers O_2 sensitivity on the SH protein.

O_2 sensitivity is also induced by a leucine modification of H396, a strictly conserved residue in motif L4. The *D. gigas* crystal structure revealed that the corresponding residue (H468) is located in the vicinity of the CO ligand (Fig. 4B; distance from Nε to O, 6.5 Å) separated by 10 Å from the Ni (distance from Nε to Ni, 10.3 Å; distance from Nε to Fe, 8.6 Å). A phenotype similar to that of the H396L mutant was observed with the T415V N419H replacement. T415 is a nonconserved residue probably corresponding to S486 in *D. gigas*, which forms a hydrogen bond to the CN1 ligand (41). In future studies infrared spectroscopy combined with biochemical analysis of the purified class IV mutant proteins will show if alterations of the diatomic ligands at the SH active site account for the increased O_2 sensitivity.

ACKNOWLEDGMENTS

We thank R. Kräft and G. Winter (HU Berlin) for excellent technical assistance and E. Schwartz for critical reading of the manuscript.

This work was funded by the European Union biotechnology program ("Structural Biology" [area 6] PL970 280), the Deutsche Forschungsgemeinschaft (SFB 498, TP C1, and SPP1070), and the Fonds der Chemischen Industrie. A. L. De Lacey thanks the Spanish Ministry of Science and Technology for a "Ramon y Cajal" contract and for funding of the work (BQU2000-0991).

REFERENCES

1. **Adams, M. W.** 1990. The structure and mechanism of iron-hydrogenases. Biochim. Biophys. Acta **1020:**115–145.
2. **Albracht, S. P. J., and R. Hedderich.** 2000. Learning from hydrogenases: location of a proton pump and of a second FMN in bovine NADH-ubiquinone oxidoreductase (complex I). FEBS Lett. **485:**1–6.
3. **Albracht, S. P. J.** 1994. Nickel hydrogenases: in search of the active site. Biochim. Biophys. Acta **1188:**167–204.
4. **Bagley, K. A., C. J. Van Garderen, M. Chen, E. C. Duin, S. P. J. Albracht, and W. H. Woodruff.** 1994. Infrared studies on the interaction of carbon monoxide with divalent nickel in hydrogenase from *Chromatium vinosum*. Biochemistry **33:**9229–9236.
5. **Bradford, M. M.** 1976. A rapid and sensitive method for the quantitation of microgram quantities of protein utilizing the principle of protein-dye binding. Anal. Biochem. **72:**248–254.
6. **Buhrke, T., and B. Friedrich.** 1998. *hoxX* (*hypX*) is a functional member of the *Alcaligenes eutrophus hyp* gene cluster. Arch. Microbiol. **170:**460–463.
7. **Casalot, L., and M. Rousset.** 2001. Maturation of the [NiFe] hydrogenases. Trends Microbiol. **9:**228–237.
8. **Dernedde, J., T. Eitinger, N. Patenge, and B. Friedrich.** 1996. *hyp* gene products in *Alcaligenes eutrophus* are part of a hydrogenase maturation system. Eur. J. Biochem. **235:**351–358.
9. **Eberz, G., C. Hogrefe, C. Kortlüke, A. Kamienski, and B. Friedrich.** 1986. Molecular cloning of structural and regulatory hydrogenase genes (*hox*) of *Alcaligenes eutrophus* H16. J. Bacteriol. **168:**636–641.
10. **Fontecilla-Camps, J. C., M. Frey, E. Garcin, Y. Higuchi, Y. Montet, Y. Nicolet, and A. Volbeda.** 2001. Molecular architectures, p. 101–107. *In* R. Cammack, M. Frey, and R. Robson (ed.), Hydrogen as a fuel. Taylor & Francis, London, United Kingdom.
11. **Friedrich, B., E. Heine, A. Finck, and C. G. Friedrich.** 1981. Nickel requirement for active hydrogenase formation in *Alcaligenes eutrophus*. J. Bacteriol. **145:**1144–1149.
12. **Garcin, E., X. Vernede, E. C. Hatchikian, A. Volbeda, M. Frey, and J. C. Fontecilla-Camps.** 1999. The crystal structure of a reduced [NiFeSe] hydrogenase provides an image of the activated catalytic center. Structure Fold. Des. **7:**557–566.
13. **Happe, R. P., W. Roseboom, G. Egert, C. G. Friedrich, C. Massanz, B. Friedrich, and S. P. J. Albracht.** 2000. Unusual FTIR and EPR properties of the H_2-activating site of the cytoplasmic NAD-reducing hydrogenase from *Ralstonia eutropha*. FEBS Lett. **466:**259–263.
14. **Happe, R. P., W. Roseboom, A. J. Pierik, S. P. Albracht, and K. A. Bagley.** 1997. Biological activation of hydrogen. Nature **385:**126.
15. **Higuchi, Y., H. Ogata, K. Miki, N. Yasuoka, and T. Yagi.** 1999. Removal of the bridging ligand atom at the Ni-Fe active site of [NiFe] hydrogenase upon reduction with H_2, as revealed by X-ray structure analysis at 1.4 Å resolution. Structure Fold. Des. **7:**549–556.
16. **Higuchi, Y., T. Yagi, and N. Yasuoka.** 1997. Unusual ligand structure in Ni-Fe active center and an additional Mg site in hydrogenase revealed by high resolution X-ray structure analysis. Structure **5:**1671–1680.
17. **Magalon, A., M. Blokesch, E. Zehelein, and A. Böck.** 2001. Fidelity of metal insertion into hydrogenases. FEBS Lett. **499:**73–76.
18. **Magalon, A., and A. Böck.** 2000. Analysis of the HypC-HycE complex, a key intermediate in the assembly of the metal center of the *Escherichia coli* hydrogenase 3. J. Biol. Chem. **275:**21114–21120.
19. **Maier, T., and A. Böck.** 1996. Ni incorporation into hydrogenases, p. 173–

192. *In* R. P. Hausinger, G. L. Eichhorn, and L. G. Marzilli (ed.), Advances in inorganic biochemistry: mechanisms of metallocenter assembly. VCH Publishers, Inc., New York, N.Y.
20. **Massanz, C., and B. Friedrich.** 1999. Amino acid replacements at the H_2-activating site of the NAD-reducing hydrogenase from *Alcaligenes eutrophus*. Biochemistry **38:**14330–14337.
21. **Massanz, C., S. Schmidt, and B. Friedrich.** 1998. Subforms and in vitro reconstitution of the NAD-reducing hydrogenase of *Alcaligenes eutrophus*. J. Bacteriol. **180:**1023–1029.
22. **Massanz, C., V. M. Fernandez, and B. Friedrich.** 1997. C-terminal extension of the H_2-activating subunit, HoxH, directs maturation of the NAD-reducing hydrogenase in *Alcaligenes eutrophus*. Eur. J. Biochem. **245:**441–448.
23. **Miller, J. H.** 1972. Experiments in molecular genetics. Cold Spring Harbor Laboratory Press, Cold Spring Harbor, N.Y.
24. **Montet, Y., P. Amara, A. Volbeda, X. Vernede, E. C. Hatchikian, M. J. Field, M. Frey, and J. C. Fontecilla-Camps.** 1997. Gas access to the active site of Ni-Fe hydrogenases probed by X-ray crystallography and molecular dynamics. Nat. Struct. Biol. **4:**523–526.
25. **Nicolet, Y., C. Piras, P. Legrand, C. E. Hatchikian, and J. C. Fontecilla-Camps.** 1999. *Desulfovibrio desulfuricans* iron hydrogenase: the structure shows unusual coordination to an active site Fe binuclear center. Structure Fold. Des. **7:**13–23.
26. **Pavlov, M., P. E. M. Siegbahn, M. R. A. Blomberg, and R. H. Crabtree.** 1998. Mechanism of H-H activation by nickel-iron hydrogenase. J. Am. Chem. Soc. **120:**548–555.
27. **Peters, J. W., W. N. Lanzilotta, B. J. Lemon, and L. C. Seefeldt.** 1998. X-ray crystal structure of the Fe-only hydrogenase (CpI) from *Clostridium pasteurianum* to 1.8 angstrom resolution. Science **282:**1853–1858.
28. **Pierik, A. J., W. Roseboom, R. P. Happe, K. A. Bagley, and S. P. J. Albracht.** 1999. Carbon monoxide and cyanide as intrinsic ligands to iron in the active site of [NiFe] hydrogenases. $NiFe(CN)_2CO$, biology's way to activate H_2. J. Biol. Chem. **274:**3331–3337.
29. **Pilkington, S. J., J. M. Skehel, R. B. Gennis, and J. E. Walker.** 1991. Relationship between NADH-ubiquinone reductase and a bacterial NAD-reducing hydrogenase. Biochemistry **30:**2166–2175.
30. **Sambrook, J., E. F. Fritsch, and T. Maniatis.** 1989. Molecular cloning: a laboratory manual, 2nd ed., Cold Spring Harbor Laboratory Press, Cold Spring Harbor, N.Y.
31. **Schneider, K., H. G. Schlegel, R. Cammack, and D. O. Hall.** 1979. The iron-sulphur centres of soluble hydrogenase from *Alcaligenes eutrophus*. Biochim. Biophys. Acta **578:**445–461.
32. **Schneider, K., and H. G. Schlegel.** 1978. Identification and quantitative determination of the flavin component of soluble hydrogenase from *Alcaligenes eutrophus*. Biochem. Biophys. Res. Commun. **84:**564–571.
33. **Schneider, K., and H. G. Schlegel.** 1976. Purification and properties of the soluble hydrogenase from *Alcaligenes eutrophus* H16. Biochim. Biophys. Acta **452:**66–80.
34. **Simon, R., U. Priefer, and A. Pühler.** 1983. A broad host range mobilization system for *in vivo* genetic engineering: transposon mutagenesis in gram-negative bacteria. Bio/Technology **1:**717–743.
35. **Thiemermann, S., J. Dernedde, M. Bernhard, W. Schroeder, C. Massanz, and B. Friedrich.** 1996. Carboxy-terminal processing of the soluble, NAD-reducing hydrogenase of *Alcaligenes eutrophus* requires the *hoxW* gene product. J. Bacteriol. **178:**2368–2374.
36. **Towbin, H., T. Staehelin, and J. Gordon.** 1979. Electrophoretic transfer of protein from polyacrylamide gels to nitrocellulose sheets: procedure and some applications. Proc. Natl. Acad. Sci. USA **76:**4350–4354.
37. **Tran-Betcke, A., U. Warnecke, C. Böcker, C. Zaborosch, and B. Friedrich.** 1990. Cloning and nucleotide sequences of the genes for the subunits of NAD-reducing hydrogenase of *Alcaligenes eutrophus* H16. J. Bacteriol. **172:**2920–2929.
38. **van der Spek, T. M., A. F. Arendsen, R. P. Happe, S. Yun, K. A. Bagley, D. J. Stufkens, W. R. Hagen, and S. P. J. Albracht.** 1996. Similarities in the architecture of the active sites of Ni-hydrogenases and Fe-hydrogenases detected by means of infrared spectroscopy. Eur. J. Biochem. **237:**629–634.
39. **van der Zwaan, J. W., J. M. C. C. Coremans, E. C. M. Bouwens, and S. P. J. Albracht.** 1990. Effect of $^{17}O_2$ and ^{13}CO on EPR spectra of nickel in hydrogenase from *Chromatium vinosum*. Biophys. Biochim. Acta **104:**101–110.
40. **Vignais, P. M., B. Billoud, and J. Meyer.** 2001. Classification and phylogeny of hydrogenases. FEMS Microbiol. Rev. **25:**455–501.
41. **Volbeda, A., E. Garcin, C. Piras, A. L. De Lacey, V. M. Fernandez, E. C. Hatchikian, M. Frey, and J. C. Fontecilla-Camps.** 1996. Structure of the [NiFe] hydrogenase active site: evidence for biologically uncommon Fe-ligands. J. Am. Chem. Soc. **118:**12989–12996.
42. **Volbeda, A., M.-H. Charon, C. Piras, E. C. Hatchikan, M. Frey, and J. C. Fontecilla-Camps.** 1995. Crystal structure of the nickel-iron hydrogenase from *Desulfovibrio gigas*. Nature **373:**580–587.
43. **Voordouw, G.** 1992. Evolution of hydrogenase genes. Adv. Inorg. Chem. **38:**397–422.
44. **Wolf, I., T. Buhrke, J. Dernedde, A. Pohlmann, and B. Friedrich.** 1998. Duplication of *hyp* genes involved in maturation of [NiFe] hydrogenases in *Alcaligenes eutrophus* H16. Arch. Microbiol. **170:**451–459.
45. **Wu, L. F., and M. A. Mandrand.** 1993. Microbial hydrogenases: primary structure, classification, signatures and phylogeny. FEMS Microbiol. Rev. **10:**243–269.